

Physics-Based Phase Noise Analysis of CMOS RF Oscillators

Sung-Min Hong, Chan Hyeong Park*, Myoung Jin Lee, Hong Shick Min, and Young-June Park

School of Electrical Engineering and Computer Science and NSI-NCRC,

Seoul National University, San 56-1, Sillim-dong, Gwanak-gu, Seoul 151-744, Korea

Tel : +82-2-880-7285, Fax : +82-2-882-4658, E-mail : hi2ska2@isis.snu.ac.kr

* Dept. of Electronics and Communications Eng., Kwangwoon University, Seoul 139-701, Korea

Abstract—A TCAD framework that can predict the phase noise spectrum of the oscillator using the nonlinear perturbation analysis is developed. The device-circuit mixed-mode simulation technique based upon the shooting-Newton method is exploited to evaluate the periodic steady-state solution of the oscillator. The influence of noise sources inside the devices on the phase deviation is calculated in an efficient and accurate way using the perturbation projection vector. The output power spectrum can be easily obtained in this framework. As its application, the output power spectrum of a CMOS LC voltage-controlled oscillator is calculated.

I. INTRODUCTION

An accurate phase noise simulation of CMOS RF oscillators is very important to design low-noise CMOS RF communication systems. In this work, we have developed a comprehensive TCAD framework that can predict the phase noise spectrum of the oscillator using the nonlinear perturbation analysis [1]. The device-circuit mixed-mode simulation technique based upon the shooting-Newton method has been exploited to obtain the periodic steady-state solution of the oscillator. With this framework, the influence of noise sources inside the devices on the oscillator phase noise spectrum can be calculated in an efficient and accurate manner by the use of the perturbation projection vector. The output power spectrum can be easily obtained in this framework.

II. DEVICE-CIRCUIT MIXED-MODE SIMULATION FOR OSCILLATORS

We consider a circuit system consisting of M semiconductor devices and L lumped circuit elements. A lumped circuit element can be fully characterized by the relationship between its terminal voltages and currents. The semiconductor equations (Poisson's equation and continuity equations for electrons and holes) with the appropriate boundary conditions for each device in the circuit are discretized as in the conventional device simulators. Then the state variables for the system are the electrostatic potential, the electron density, and the hole density at each node of the spatially discretized devices, and the terminal voltages and currents of both the semiconductor devices and the lumped circuit elements. The total number of the state variables is denoted by N_{tot} .

The state equations for the state variables are the semiconductor equations for the devices, the constitutive equations

for the lumped elements, and the Kirchhoff's current law (KCL). If we write the state variables as $x(t)$ in a vector form, these N_{tot} state equations can be written as follows [2]:

$$\frac{d}{dt}Q(x) + J(x) = b_{ext}(t) + b_n(t), \quad (1)$$

where t is the time, $b_{ext}(t)$ is a vector for the externally applied voltage (or current) sources, and $b_n(t)$ is a vector representing the noise sources. $Q(x)$ and $J(x)$ are usually nonlinear functions.

Now, let us find $x_s(t)$ that is a periodic steady-state solution without the noise source vector $b_n(t)$, i.e.,

$$\frac{d}{dt}Q(x_s(t)) + J(x_s(t)) = b_{ext}. \quad (2)$$

The shooting-Newton method is an iterative procedure layered on top of transient analysis, which is designed to solve the following boundary-value problem,

$$x_s(T_0) - x_s(0) = 0, \quad (3)$$

where T_0 is the oscillation period. After the transient simulation during the time interval T_0 is performed, an update vector for $x_s(0)$ is calculated by solving (3) with Newton's method, and this procedure is repeated until the initial value $x_s(0)$ and the final value $x_s(T_0)$ become eventually identical. In this work, the “matrix-free” shooting-Newton method [3], where an iterative matrix solver GMRES [4] is used, is implemented to find $x_s(t)$. In the oscillator, the oscillation frequency cannot be determined *a priori* before the simulation. Thus the oscillation period T_0 is added to the state variables and an additional “phase-fixing” equation is also introduced in the state equations [5].

III. NONLINEAR PERTURBATION ANALYSIS OF OSCILLATOR NOISE

We consider the perturbed solution $x(t)$ from the unperturbed solution $x_s(t)$ by the influence of the noise source vector $b_n(t)$. Since there is no perfect time reference in the oscillators, the vector for the state variables $x_s(t + t_0)$, which is shifted from $x_s(t)$ by an amount of time interval t_0 , is also another periodic steady-state solution. Therefore, for the noise simulation of the oscillator, an additional “phase deviation”

term $\alpha(t)$ should be introduced, and the perturbed solution $x(t)$ is expressed by [6]

$$x(t) = x_s(t + \alpha(t)) + y(t + \alpha(t)), \quad (4)$$

where $y(t + \alpha(t))$ is the “small” orbital deviation, often neglected in phase noise analysis [1], [7].

We use the following equation and the boundary condition for $\alpha(t)$, which is widely accepted to be most suitable for many applications [8]:

$$\frac{d}{dt}\alpha(t) = v_1^T(t + \alpha(t))B(x_s(t + \alpha(t)))b_w(t), \quad (5)$$

$$\alpha(0) = 0, \quad (6)$$

where the instant $t = 0$ is chosen to be the beginning of the perturbation and $B(x_s(t + \alpha(t)))b_w(t)$ represents the noise sources. The perturbation projection vector (PPV) [9], $v_1(t)$, is a T_0 -periodic real vector, which represents the effects of the noise sources on the phase deviation. The PPV determines the component of the noise sources which aligns with the persistent eigen-mode [10]. Only this component is known to contribute to the phase noise of the oscillator [1], [6]. We implemented the algorithm in [9] to evaluate $v_1(t)$ mainly because it is consistent to the procedure used to calculate the periodic steady-state solution in this work.

If z is the output variable and f is the observation frequency, the power spectrum of $z(t+\alpha(t))$ can be determined as follows [1]:

$$S_z(f) = 2 \sum_{i=-\infty}^{\infty} Z_i Z_i^* \frac{f_0^2 i^2 c}{\pi^2 f_0^4 i^4 c^2 + (f + i f_0)^2}, \quad (7)$$

where f_0 is the oscillation frequency, and Z_i is the i -th Fourier coefficient of $z_s(t)$. When we consider the diffusion noise sources in the devices and thermal noise sources for the resistors, the scalar c in (7) can be calculated by

$$c = \sum_{m=1}^M \frac{1}{T_0} \int_0^{T_0} dt \left(\sum_{\beta=n,p} \int_{\Omega_m} d\mathbf{r} |\nabla v_{1,\beta}^m(\mathbf{r},t)|^2 K_{\xi_\beta, \xi_\beta}^m(\mathbf{r},t) \right) + \sum_{l=1}^{L_r} \frac{1}{T_0} \int_0^{T_0} dt (v_1^l(t))^2 K_{\xi, \xi}^l, \quad (8)$$

where $K_{\xi_\beta, \xi_\beta}^m(\mathbf{r},t)$ is the magnitude of the diffusion noise source in the m -th device and $K_{\xi, \xi}^l$ is the magnitude of the thermal noise source in the l -th resistor.

IV. NUMERICAL EXAMPLE AND DISCUSSION

A cross-coupled CMOS LC VCO shown in Fig. 1 has been simulated. The oscillator is designed to have a tuning range from 500 MHz to 900 MHz. All of the dimensions for the MOSFETs and the values for the circuit components are shown in the figure. The output signal is taken as a differential voltage between the drain terminals (V_{out}^- and V_{out}^+) of $M1$ and $M2$. Two NMOSFETs ($M1$ and $M2$), one PMOSFET ($M3$), and two MOS varactors ($VC1$ and $VC2$) are treated

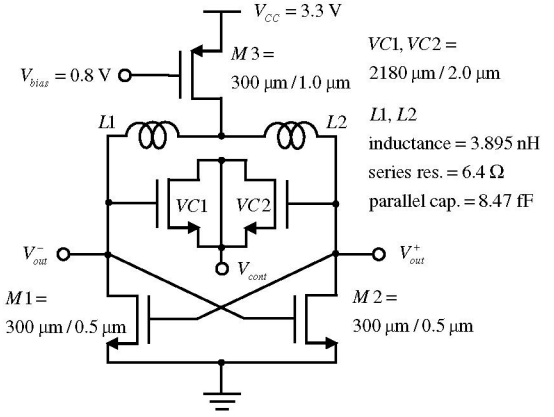


Fig. 1. Schematic of a cross-coupled CMOS LC VCO.

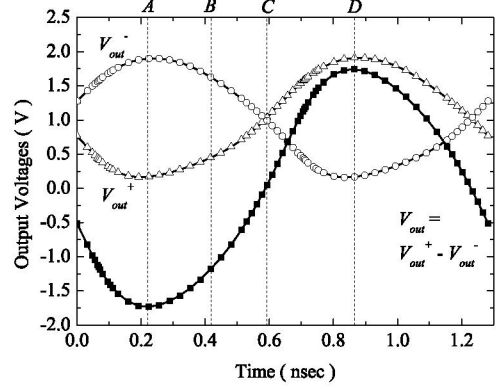


Fig. 2. Output voltage waveforms of the simulated periodic steady-state solution when V_{cont} is 1.0 V and V_{bias} is 0.8 V.

by the two-dimensional semiconductor devices. Two inductors ($L1$ and $L2$) are characterized by inductance, series resistance, and parallel capacitance. The inductors have the same quality factor about 3 at 780 MHz. N_{tot} is set to be 53,020.

Fig. 2 shows the output voltage waveforms of the simulated periodic steady-state solution when V_{cont} is 1.0 V and V_{bias} is 0.8 V. In this bias condition, the oscillation frequency of the LC VCO, f_0 , is found to be 780 MHz. To obtain the periodic steady-state solution, 64 nonuniform sampling time points are generated during a period in transient simulation. We will concentrate on four time instants A , B , C , and D in Fig. 2 in the following discussion. At A and D , either $M1$ or $M2$ is turned on, and the other is turned off. At C , two NMOSFETs are balanced because V_{out}^+ and V_{out}^- have same value. B is the mid-point between A and C . Electron densities at the oxide-silicon interface of $M1$ are plotted at the four time instants in Fig. 3. Note that K_{ξ_n, ξ_n}^{M1} is proportional to the electron density.

We have performed the PPV calculation using the information for the periodic steady-state solution. Fig. 4 shows the PPVs for the electron continuity equation, in unit of

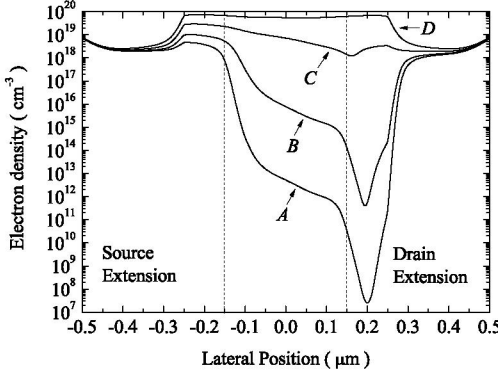


Fig. 3. Electron densities at the oxide-silicon interface of $M1$.

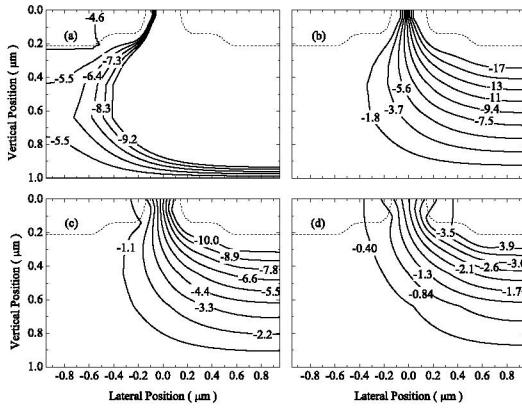


Fig. 4. PPVs for the electron continuity equation, in unit of A^{-1} , in the silicon substrate of $M1$ at the four time instants, (a) A , (b) B , (c) C , and (d) D . Nine contours with uniform steps between the maximum value and minimum value are generated for each time. The dashed lines denote the metallurgical junctions. The gate contact is located from $-0.25 \mu m$ to $0.25 \mu m$ in the lateral position. The zero point in the vertical position is the oxide-silicon interface.

A^{-1} , in the silicon substrate of $M1$ at the four time instants. When $M1$ is biased under the subthreshold condition (A), the PPV along the MOSFET channel has a very sharp gradient only at near-source region. As the gate voltage of $M1$, V_{out}^+ , increases (B), the PPV has an almost uniform distribution along the MOSFET channel. When even higher gate voltage is applied (C and D), the gradient of the PPV appears also in the source/drain extension. On the other hand, the PPVs for electron continuity equation, in unit of A^{-1} , in the silicon substrate of $VC1$ at the four time instants, which are shown in Fig. 5, have different shapes. The PPV in $VC1$ has its maximum (or minimum) value near the mid-point of the gate, and small values at the source, drain, and substrate region. By symmetry, the gradient of the PPV has zero value at the mid-point of the gate, and the peak position of $\nabla v_{1,n}^{VC1}$ moves slightly as the gate voltage changes.

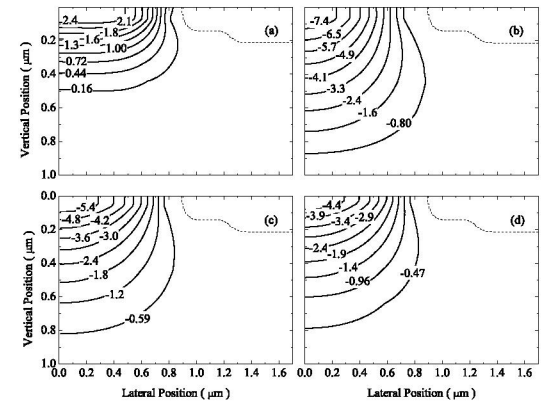


Fig. 5. PPVs for the electron continuity equation, in unit of A^{-1} , in the silicon substrate of $VC1$ at the four time instants, (a) A , (b) B , (c) C , and (d) D . By symmetry, only half of the varactor is shown in this figure. Nine contours with uniform steps between the maximum value and minimum value are generated for each time. The dashed lines denote the metallurgical junctions. The gate contact is located from $-1 \mu m$ to $1 \mu m$ in the lateral position. The zero point in the vertical position is the oxide-silicon interface.

Fig. 6 shows the spatial distribution of c originated from the electron diffusion noise sources in $M1$. The spatial distribution of c has its peak value at near-source region in the channel mainly because the magnitude of the noise source, K_{ξ_n, ξ_n}^{M1} , at near-source region is larger than that at near-drain region, as shown in Fig. 3. Also the spatial distribution of c originated from the electron diffusion noise sources in $VC1$ is shown in Fig. 7. Since the gradient of the PPV vanishes at the mid-point of the gate, the spatial contribution also vanishes at that point. Fig. 8 shows the contributions of the devices and the inductor losses to c as a function of time. The contribution of $M1$ to c at D is relatively small because the PPV for the electron continuity equation shows the gradual change at that instant. In this example, we can find that the contributions of the NMOSFETs ($M1$ and $M2$) to c are dominant. Averaging these contributions over a period, the value of c is found to be 0.51 fsec .

In Fig. 9, the calculated power spectral density of the output differential voltage is shown for first four harmonics of f_0 . As shown in the inset of the figure, the simulation predicts a Lorentzian shape of the phase noise spectrum. Thus it can be observed that the $1/f^2$ spectrum originates from the white noise source. At 500 kHz offset frequency, the phase noise of -92.0 dBc/Hz is obtained.

V. CONCLUSION

The physics-based phase noise analysis and simulation of the oscillators was reported and the phase noise spectrum of a CMOS LC VCO was calculated. We described the shape of the PPVs and the spatial contribution to c inside a MOSFET and a MOS varactor at a few time instants. The output power spectral density originated from the diffusion noise sources in the semiconductor devices and the thermal noise sources in

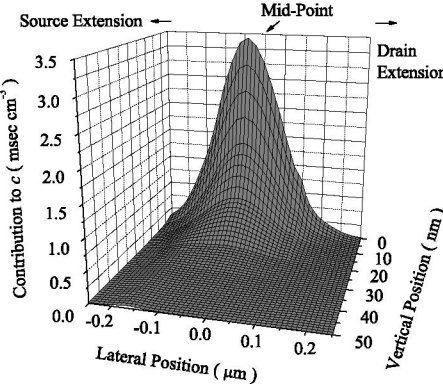


Fig. 6. Spatial distribution of c originated from the electron diffusion noise sources in $M1$. It has its peak value at the near-source region in the channel. The zero point in the lateral position is the mid-point of the gate.

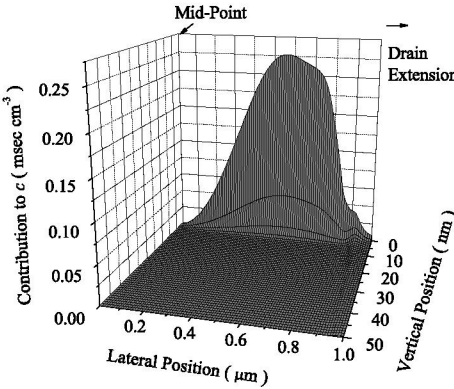


Fig. 7. Spatial distribution of c originated from the electron diffusion noise sources in VCI . By symmetry, only half of the varactor is shown in this figure. The zero point in the lateral position is the mid-point of the gate.

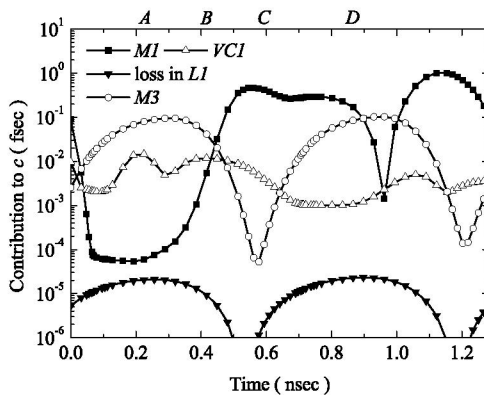


Fig. 8. Contributions of the devices and the inductor losses to c as a function of time. The contributions of $M2$ and $VC2$ can be obtained by shifting the contributions of $M1$ and VCI , respectively, by amount of $\frac{1}{2}T_0$.

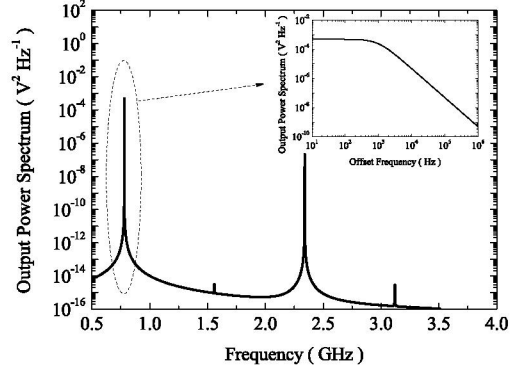


Fig. 9. Power spectral density of the output differential voltage for first four harmonics of f_0 . Inset is a blown up version of the power spectral density around the first harmonic. At 500 kHz offset frequency, the phase noise of -92.0 dBc/Hz is obtained.

the resistors shows a Lorentzian shape and can explain $1/f^2$ phase noise spectrum. We expect that this framework can be a useful tool for an accurate noise analysis in the oscillators.

ACKNOWLEDGEMENT

This work was supported by the NCRC program of the KOSEF through the NSI at Seoul National University and Samsung Electronics Company (0414-20050009 and 0414-20050037). C. H. Park's work has been supported partly by the MIC, Korea, under the ITRC support program supervised by the IITA and partly by Nano IP/SoC Promotion Group of Seoul R&BD Program in 2006.

REFERENCES

- [1] A. Demir, A. Mehrotra, and J. Roychowdhury, "Phase noise in oscillators: A unifying theory and numerical methods for characterization," *IEEE Trans. Circuits Syst. I*, vol. 47, pp. 655–674, 2000.
- [2] B. Troyanovsky, "Frequency domain algorithms for simulating large signal distortion in semiconductor devices," Ph.D. dissertation, Stanford Univ., Stanford, CA, Nov. 1997.
- [3] R. Telichevesky, K. S. Kundert, and J. K. White, "A time-domain method for numerical noise analysis of oscillators," in *Design Automation Conference*, 1995, pp. 480–484.
- [4] Y. Saad and M. H. Schultz, "GMRES: A generalized minimal residual algorithm for solving nonsymmetric linear systems," *SIAM Journal of Scientific and Statistical Computing*, vol. 7, pp. 856–869, 1986.
- [5] K. S. Kundert, "Introduction to RF simulation and its application," *IEEE J. Solid-State Circuits*, vol. 34, pp. 1298–1319, 1999.
- [6] F. X. Kaertner, "Analysis of white and $f^{-\alpha}$ noise in oscillators," *International Journal of Circuit Theory and Applications*, vol. 18, pp. 485–519, 1990.
- [7] A. Hajimiri and T. H. Lee, "A general theory of phase noise in electrical oscillators," *IEEE J. Solid-State Circuits*, vol. 33, pp. 179–194, 1998.
- [8] P. Vanassche, G. Gielen, and W. Sansen, "On the difference between two widely publicized methods for analyzing oscillator phase behavior," in *International Conference on Computer-Aided Design*, 2002, pp. 229–233.
- [9] A. Demir and J. Roychowdhury, "A reliable and efficient procedure for oscillator PPV computation, with phase noise macromodeling applications," *IEEE Trans. Computer-Aided Design*, vol. 22, pp. 188–197, 2003.
- [10] A. Demir, "Oscillator noise analysis," in *International Conference on Noise and Fluctuations*, 2005, pp. 499–504.